A Deep Water Dispersion Experiment in the Gulf of Mexico

Thomas Meunier[1], Paula Pérez Brunius[2], Javier Rodríguez Outerelo[2], Paula García Carrillo[2], Argelia Ronquillo[2], Heather Furey[1], Andrée Ramsey[1]and Amy Bower[1]

[1]Physical Oceanography Department, Woods Hole Oceanographic Institution, Woods Hole, MA, USA

[2]Departamento de Oceanografía, Centro de Investíagacion Cientifica y de Educación Superior de Ensenada, Ensenada, B.C., MEXICO

Key Points:

- Pairs of surface drifters and RAFOS floats drifting at 300 and 1500 dbar were released simultaneously in the Gulf of Mexico between 2016 and 2018.
- Relative diffusivity at 300 and 1500 dbar is on average 2 and 5 times weaker than at the surface, respectively.
- The size of energy-containing eddies appears to be about three times smaller at 1500 dbar than near the surface.

Corresponding author: T. Meunier, tmeunier@whoi.edu

Abstract

The 2010 Deep Water Horizon oil spill has dramatically impacted the Gulf of Mexico's marine environment from the sea-floor to the surface. While dispersion of contaminants at the surface has been extensively studied over the past decades, little is known about the deep water dispersion properties of the ocean, and the fate of deep contaminants is uncertain. This paper describes the results of the Deep Water Dispersion Experiment (DWDE) that took place in the western Gulf of Mexico, a deep water drilling operation area. The experiment consisted in the simultaneous release of triplets of surface drifters and RAFOS floats drifting at 300 and 1500 dbar, to assess the variations of dispersion properties with depth for the first time. Our results show that surface absolute diffusivity in the western GoM is elevated (comparable in magnitude with that of intense equatorial and western boundary currents). Diffusivity decreases with depth, and is, on average 2 times smaller (range [1-5] times) at 300 dbar and 5 times (range [3-12] times) smaller at 1500 dbar. We show that the separation scale dependence of relative diffusivity follows a Richardson's law ($K \propto D^{4/3}$) at all depths. The time dependence of relative dispersion suggests a Richardson regime near the surface and a mixed Richardson/ballistic regime in depth at scales of O(10-100 km). Analysis of the Finite Scale Lyapunov Exponents and of the pair separation's Kurtosis suggests the existence of a non-local (Lundgren) regime at separation scales smaller than the first baroclinic Rossby radius (≈50km) near the surface, and at scales smaller than O(15 km) in depth. This suggests that the size of the most energetic eddies decreases with depth. Finally, we find that in the long time limit, the dispersion regime shifts towards standard diffusion (Rayleigh regime), and is affected by the basin's boundaries, as the Kurtosis is indicative of saturated dispersion after O(100 days).

1 Introduction

The theory of particle dispersion in 2-dimensional turbulent flows [*Batchelor*, 1952; *Kraichnan*, 1967; *Lin*, 1972; *Lundgren*, 1981; *Bennett*, 1987; *Babiano et al.*, 1990; *LaCasce*, 2008] has provided a solid background for the study of passive tracers evolution in the ocean. Lagrangian experiments, releasing large numbers of tracked drifting buoys by pairs or triplets, and studying their relative movement as turbulent advection separates them, have successfully applied these concepts to reveal the turbulent regimes occurring over a variety of time and space scales in the ocean (*Colin de Verdiere* [1983]; *Davis* [1991]; *LaCasce and Bower* [2000]; *Ollitrault et al.* [2005]; *LaCasce and Ohlmann* [2003];

Zavala Sansón [2015] among many). Beyond the fundamental purpose of better understanding the nature of oceanic turbulence, the study of relative dispersion has direct applications in a number of essential biological, environmental and economical issues, from the distribution of plankton patches [*Bennett and Denman*, 1985], the dispersal of fish larvae [*Mariani et al.*, 2007], the fate of plastic waste in the ocean [*van Sebille et al.*, 2012], and the evolution of contaminant spills [*North et al.*, 2011]. While most of these problems are confined to the surface mixed layer, the recent Deep Water Horizon catastrophe in the Gulf of Mexico, discharging 650.000 m^3 of oil at a depth of 1200 m [*Kujawinski et al.*, 2011; *McNutt et al.*, 2012], showed the necessity of understanding dispersion properties of the full water column: oil is composed of a variety of constituents evolving into droplets of different sizes [*Reddy et al.*, 2012], each reaching a different neutral buoyancy depth before dispersing, and resulting in a series of distinct plumes from the sea-floor to the surface [*North et al.*, 2011]. The development of deep sea mining, involving the injection of contaminants and sediments into the water column has also recently raised concerns on the necessity of an in-depth assessment of the deep and intermediate dispersion properties of the ocean [*Drazen et al.*, 2020].

Thanks to the early work of *LaCasce and Ohlmann* [2003], and the extensive Lagrangian experiments carried out after the Deep Water Horizon spill, such as the Grand Lagrangian Deployment (GLAD [*Poje et al.*, 2014, 2017; *Beron-Vera and LaCasce*, 2016]), surface dispersion properties of the northern and western GoM are well documented. The latter was shown to be local at scales of O([10-100 km]) (Richardson regime), while its small time and spatial scale behaviour is more ambiguous: while *LaCasce and Ohlmann* [2003] and *Beron-Vera and LaCasce* [2016] reported non-local dispersion (Lundgren regime) at times shorter than a few days and separations smaller than the first Rossby radius, *Poje et al.* [2014] found a Richardson regime down to the smallest resolved scales ($\approx$ 1 km), consistent with local dispersion by energetic submesoscale structures. At these scales, *Balwada et al.* [2016] showed that dispersion was driven by divergent (ageostrophic) motion while rotational motion is responsible for the larger scale dispersion.

Despite this exceptional Lagrangian sampling effort in the surface GoM, direct observations of relative dispersion at depth are lacking. More generally, observations of deep ocean dispersion are rare. Notable exceptions include the work of *LaCasce and Bower* [2000] who studied the dispersion of RAFOS and SOFAR floats drifting between 400 and 1300 dbar in the North Atlantic and *Ollitrault et al.* [2005] who used 700 dbar SO-

FAR floats in the same oceanic basin. While both clearly identified a Richardson regime at scales ranging between 40 and 300 km, the existence of an exponential regime at small scale at these depths remained uncertain, possibly due to the relatively large initial separations of float pairs. Deep lateral diffusivity was also estimated by *LaCasce et al.* [2014] using isopycnal RAFOS floats in the Antarctic circumpolar current. Using a numerical model validated from the RAFOS observations at ≈1000 m depth, they showed that mixing was maximum at depths between 1500 and 2000 m.

As part of the Gulf of Mexico Research Consortium (CIGoM) project -a large community effort funded by the Mexican Government to better understand the dynamics of the GoM and its response to oil spills, the Deep Water Dispersion Experiment (DWDE) was designed to simultaneously measure the deep, intermediate, and surface dispersion properties of the Perdido region in the western GoM. The Perdido region, located across Mexico and USA's exclusive economic zones, is a particularly sensible region, as it shelters some of the world's deepest drilling operations, at about 200 miles from the Texas and Tamaulipas shores. The experiment, performed in 4 legs between June 2016 and November 2018, consisted in the simultaneous release of surface drifters and RAFOS floats drifting at 300 and 1500 dbar, to assess and compare the water column's dispersion properties. To our knowledge, this is only the second experiment of simultaneous release of drifter clusters at different depths (see *Balwada et al.* [2019] for an experimental study of dispersion at two different depth ranges in the Southern Ocean), so that, beyond the essential environmental necessity of studying deep dispersion in the western GoM, the DWDE experiment provides one of the first direct observations of the depth dependence of dispersion and diffusivity.

2 Data

The surface drifters and RAFOS floats deployment site is shown on figures 1c,d,e. Surface drifters drogued at 1 m, and RAFOS floats drifting at 300 and 1500 dbar, were released simultaneously as triplets (each triplet corresponding to 3 pairs). Each triplet was separated by 50 km in the cross-slope direction. The sampling rate of surface drifters (1 hour) was degraded to the RAFOS floats 8 hour rate for consistency of the data sets. This results in a partial filtering of inertial oscillations, which were shown to affect scale-dependent variables such as Finite Size Lyapunov Exponents at scales of a few kilometres [*Beron-Vera and LaCasce*, 2016]. The parking depths of the RAFOS floats were chosen

to represent the top and deep layers of the GoM, whose circulation is essentially two-layered [*Hamilton et al.*, 2018]. Positioning of the RAFOS floats was performed using an array of 5 sound sources deployed prior to the experiments. From a total of 84 recovered RAFOS floats (44 at 300 dbar and 40 at 1500 dbar), 51 completed a full mission, while 33 surfaced earlier, most likely due to attacks by large pelagic fish. These early risers were almost entirely 300 dbar floats, resulting in an incomplete data set and weaker statistical significance of the results at this depth. The dataset used in the present study is composed of 207 original pairs of surface drifters, 37 pairs of 300 dbar RAFOS floats, and 40 pairs of 1500 dbar RAFOS floats. We also included chance pairs, which are floats that were not initially launched together, but approached one another by chance [*Morel and Larceveque*, 1974; *LaCasce and Ohlmann*, 2003], resulting in a total number of 294, 39, and 43 pairs for the surface, 300 dbar, and 1500 dbar datasets, respectively. While the number of RAFOS pairs is small compared to typical surface drifter experiments, yielding a higher level of uncertainty, it should be mentioned that deep dispersion experiments are rare and any new information is valuable. The deployment strategy was designed to answer *Beron-Vera and LaCasce* [2016]'s concerns on the biasing effect of releasing simultaneously all pairs in the same location. To avoid undesired correlation between different pairs, instruments were released as triplets approximately 50 km apart (the average first baroclinic Rossby radius in the GoM), during four release campaigns 6 months apart. Details of the floats life cycles, including launch and surface dates are available as supplementary information (Fig. SI.1), as well as a detailed map of the deployment sites and sound sources array (Fig. SI.2).

3 Methods

Important theoretical efforts in Lagrangian fluid dynamics since the early fifties (e.g. *Batchelor* [1952]; *Lundgren* [1981]; *Bennett* [1987]; *Babiano et al.* [1990]; *Artale et al.* [1997]) provided an arsenal of diagnoses that allow us to discriminate between turbulent regimes. The variables used in the present study were extensively described and discussed in a number of reviews (e.g. *Davis* [1991]; *LaCasce* [2008]) and their definitions and properties are only briefly recalled below:

The separation vector $\vec{D}$ between two particles whose Lagrangian coordinates at time t are $\vec{a}_1$ and $\vec{a}_2$ is defined as:

$$\vec{D}(t, \vec{D}_0) = \vec{D}_0 + \vec{A}(\vec{a}_1, t) - \vec{A}(\vec{a}_2, t), \tag{1}$$

where $\vec{D}_0$ is the initial separation vector, and $\vec{A}(\vec{a}_i, t)$ is the absolute displacement vector of particle i at time t. In this work, initial separation is chosen to be 6 km, which corresponds to the error margin of the RAFOS acoustic positioning. Relative dispersion is defined as the ensemble mean at time t of the squared norm of the separation vectors of all particle pairs that were originally separated by a distance $D_0 = \|\vec{D}_0\|$:

$$D^2(t, D_0) = \langle \vec{D}(t, \vec{D}_0) \cdot \vec{D}(t, \vec{D}_0) \rangle. \tag{2}$$

Considering a tracer patch as a large number of individual particles, relative dispersion can be thought of as a proxy of the instantaneous area of a patch whose initial area was D_0^2. Relative diffusivity is a measure of the rate of change of this area with time, or spreading, and is defined as:

$$K(t, D_0) = \frac{1}{2} \frac{d}{dt} D^2(t, D_0). \tag{3}$$

Relative diffusivity is a scale dependent variable, and the relationship between $K(t, D_0)$ and the separation scale $\|\vec{D}(t)\|$ is an important indicator of the turbulent regime. In the Richardson's regime, where dispersion is driven by eddies that are the same scale as pair separation (local regime), diffusivity is expected to grow as $K(D) \propto D^{4/3}$ [*Batchelor*, 1952; *LaCasce*, 2008]. In the Lundgren (or Lin) regime, where dispersion is driven by eddies that are larger than pair separation (non-local regime), diffusivity is expected to grow as $K(D) \propto D^2$ [*Lin*, 1972; *Lundgren*, 1981; *Beron-Vera and LaCasce*, 2016]. These different regimes are directly linked to the Eulerian kinetic energy (KE) spectrum: the Richardson regime is found at scales larger than the energy-containing eddies, where energy cascades towards larger scales and the KE spectrum slopes as $k^{-5/3}$, while the Lundgren regime is expected at scales that are smaller than the energy-containing eddies, which corresponds to a direct enstrophy cascade and a KE spectrum that is steeper than k^{-3} [*Kraichnan*, 1967]. Similarly, the time dependence of dispersion provides information on the turbulent regime, with typical growth laws of $D^2 \propto t^3$ and $D^2 \propto e^{\gamma t}$ (where γ is the exponential growth rate, or inverse e-folding time) for the local and non-local regimes, respectively.

When using a limited number of particle pairs (as is the case in the DWDE experiment), or sampling regions of the ocean where the 2D turbulence theory's hypothesis (stationary and isotropic turbulence in an infinite domain) do not hold, as is the case for the semi-enclosed Gulf of Mexico, the fundamental relations between dispersion and time, or between relative diffusivity and separation, can eventually be uncertain or contradic-

tory [*Artale et al.*, 1997; *Beron-Vera and LaCasce*, 2016; *LaCasce*, 2008]. A number of Lagrangian diagnoses can then help to distinguish between the possible regimes.

In particular, we will make use of the finite size Lyapunov exponent (FSLE) [*Artale et al.*, 1997; *LaCasce and Ohlmann*, 2003], which is a measure of the (inverse) average time necessary for pair separation to increase by a chosen factor α. The computation procedure consists in selecting a series of pair separation distances D_i growing as $D_{i+1} = \alpha D_i$, and averaging the finite time T_i necessary for separation distance to grow from D_i to D_{i+1}. The FSLE is then defined as :

$$\lambda = ln(\alpha)\langle T_i \rangle^{-1}, \tag{4}$$

where the ensemble averaging is performed on each separation distance D_i. Because FSLEs are defined in terms of spatial rather than temporal scales, they are particularly suited for the study of dispersion in closed basins where the size of the eddies is not very small compared to the size of the domain [*Artale et al.*, 1997]. Also, FSLE does not depend on the initial separation $\vec{D}_0$, so that one can use all available pairs for a given separation scale, regardless of the initial conditions [*LaCasce*, 2008]. In the Richardson's regime, FSLE decays as $\lambda \propto D^{-2/3}$, while it is constant in the Lundgren's regime ($\lambda \propto D^0$) [*LaCasce and Ohlmann*, 2003; *Balwada et al.*, 2019].

The Kurtosis of the pair separation probability density function (PDF) will also be discussed. It is the PDF's fourth moment and is a measure of the shape of the distribution [*LaCasce and Bower*, 2000; *LaCasce and Ohlmann*, 2003; *LaCasce*, 2008], defined as:

$$Ku(t) = \frac{\langle \|\vec{D}\|^4 \rangle}{\langle \|\vec{D}\|^2 \rangle^2} \tag{5}$$

In Richardson's regime, Kurtosis has a constant value of 5.6, while it grows exponentially in Lundgren's regime.

Finally, note that the Lundgren and Richardson regimes occur at finite time, when the particles are close enough so that their absolute velocities are still correlated. A third case, the Rayleigh regime, is found in the long-time asymptotic limit, as the particles separation becomes large compared to the eddies size. In that regime, while the Eulerian KE spectrum's slope remains similar to the Richardson's regime ($k^{-5/3}$), the growth of relative dispersion becomes linear, while relative diffusivity saturates at a constant value, corresponding to twice the single particle (or absolute) diffusivity [*Babiano et al.*, 1990].

4 Results

Trajectories of all surface drifters, 300 dbar and 1500 dbar RAFOS floats are shown in the spaghetti plots of Fig. 1a,b,c, respectively. The western GoM was densely sampled at all depths. Surface drifters and 1500 dbar floats travelled Eastward as far as 88°W (eastward of 88°W in the case of a few surface drifters), while the 300 dbar floats remained west of 90°W. At all depths, the westward spreading of the floats was constrained by the topography. As an analogy to a passive tracer patch, we computed the smallest convex polygons (SCP) containing the entire drifters set for the first 150 days after launching (Fig. 1d,e,f). The launch region is depicted by the black polygons. Time evolution of the growth of the SCPs is illustrative of absolute dispersion of the drifters clusters. The growth of SCPs at all depths appears to be quickly bounded to the west by the topography. After 150 days, absolute dispersion of the surface drifters is saturated by the basin's boundary, and the SCPs occupy the entire western basin, bounded by the continental shelf to the west, north and south, while it extends as far as $88°W$ in the interior GoM. At 300 dbar, SCPs grow faster in the meridional direction, closely following the 300 m isobath in the west, and only extending to $92°W$ to the east. On the contrary, the 1500 dbar SCP's growth is more zonal, as floats reach the Campeche bank after 100 days. After 150 days, the 1500 dbar floats still haven't reached the Bay of Campeche or the northern continental slope. Since the float number is not identical at all depths, and since SCPs are representative of the furthest-drifting floats, it should be stated that SCPs should not be considered as a quantitative measure of dispersion, but only as a qualitative visual illustration.

Maps of relative displacements of the drifter pairs are shown in Fig. 1g,h,i. The figure shows the distance of each drifter or float to the centre of gravity of the pair it belongs to, corresponding to the half separation ($\frac{1}{2}\|\vec{D}\|$). The difference in pair numbers is evident in these plots: the surface is sampled more densely than the 300 dbar and 1500 dbar levels (207, 37, and 40 pairs respectively). At all depths, floats disperse isotropically around the centre of gravity, reaching maximum distances of approximately 400, 300, and 200 km for the Surface, 300 dbar, and 1500 dbar floats, respectively.

Time evolution of the mean separation at each depth is shown in Fig. 2a. At the surface and at 300 dbar, separation grows regularly during the first 80 days at a similar rate. It then saturates between 250 and 300 km at 300 dbar, while it keeps on growing to reach 400 km after 150 days at the surface. At 1500 dbar, separation grows regularly during the whole period to reach 120 km after 150 days. Pair separation velocity (Fig.

2b) grows during the first 40 days and saturates at approximately 0.4 and 0.2 $m\ s^{-1}$ at the surface and 300 dbar, respectively. The growth is slower at 1500 dbar, where no threshold was reached after 150 days. At all depths, relative dispersion grows as a power function of time over a finite range of time: At the surface, it grows as $t^{2.6}$ between 5 and 25 days, while at 300 and 1500 dbar, it grows as $t^{2.4}$ and $t^{2.2}$ in the time ranges [10-50] and [8-65] days, respectively. The separation velocity variance on these time scales grows linearly with time (Fig. 2d). At longer time scales, the growth of relative dispersion becomes linear ($D^2 \propto t^1$) as the separation velocity variance saturates and its slope tends towards zero. Dispersion then seems to saturate at scales greater than 100 km. Time evolution of relative dispersion at short time scales is examined in Fig. 2e. The scale of the x-axis (time) is linear while the scale of the y-axis (dispersion) is logarithmic. No linear trend, which would be indicative of exponential growth, is evident at short times ($<$ 10 days) at any depth. The exponential growth rate of dispersion was computed as $\gamma(t) = \frac{ln(D^2(t+\delta t))-ln(D^2(t-\delta t))}{2\delta t}$ and is shown in Fig. 2f. Exponential growth periods would materialize as portions of constant $\gamma(t)$. Here, the growth rate appears to decay at all depths, without stabilizing around any particular values during the first days. Note that the error bars are large, so that the data do not allow us to definitely rule out the possibility of an exponential regime at short time.

The FSLEs at the surface, 300 dbar and 1500 dbar are plotted against separation scale in Fig. 3a. At the surface and at 300 dbar, the FSLEs are nearly constant up to separations of O(40 km), before decaying with increasing separation at larger scales. On average, the FSLEs at the surface and 300 dbar decay as $D^{-0.65}$ and $D^{-0.77}$, respectively, between 40 and 700 km, close to the Richardson's law ($D^{-2/3}$). A similar pattern is observed at 1500 dbar, with a transition at separation scales of O(15 km) between constant FSLE and a Richardson-like decay ($D^{-0.60}$).

Time evolution of the Kurtosis is shown in Fig. 3b and c. At the surface, the Kurtosis grows exponentially during the first 2 days and stabilizes around the Richardson's value (5.6). It then decays after t = 15 days and approaches 2 (indicative of the Rayleigh regime) after 50 days, and then converges towards 1.7 at longer times. A similarly fast short time growth is observed at 300 dbar during the first 5 days, saturating at a sub-Richardson value ($\approx$ 4), then decaying to reach 2 after 60 days and converging towards 1.7 at long times. Early surfacing of 300 dbar floats result in an artificial discontinuity of the Kurtosis at 90 days. The Kurtosis at 1500 dbar exhibits a distinct evolution: although

the growth rate during the first two days has the same order of magnitude as at 300 dbar, the Kurtosis keeps on growing irregularly to reach 5.6 after 30 days, and then decays to approach 2 after 135 days.

Relative diffusivity at the surface, 300 and 1500 dbar are compared in Fig. 3d. At all depths, relative diffusivity grows with increasing separation scale as $K \propto D^{4/3}$ for scales of 6 to 100 km, and then saturates to twice the single particle diffusivity ($\approx$ 23000, 9000, and 4000 $m^2\ s^{-1}$ at the surface, 300 dbar and 1500 dbar, respectively). To assess the decrease of relative diffusivity with depth, we computed the ratio of relative diffusivity at 300 and 1500 dbar over the surface diffusivity (Fig. 3e). Relative diffusivity were first averaged over 5 km separation bins ranging from 5 to 300 km. At all resolved scales, relative diffusivity decreases with depth. Although uncertainties are large, we found that relative diffusivity is respectively 1 to 5 times (average of 2) and 3 to 12 times (average of 5) smaller at 300 and 1500 dbar than at the surface. No evident scale dependence of the diffusivity ratio could be found, given the large noise levels.

5 Discussion and conclusion

Values of the asymptotic saturation of surface relative diffusivity at scales larger than O(100 km) appear to belong to the high end of the World ocean's observed range. *Zhurbas and Oh* [2004]'s atlas of surface drifter based absolute diffusivity shows that values larger than O($10^4 m^2\ s^{-1}$), similar to our estimates of the surface GoM, are only reached in the equatorial currents, north of the subtropical gyres, and in the western boundary currents and their offshore extensions. Our estimates are however of the same order of magnitude as *Koszalka et al.* [2009]'s observations in the Nordic seas (O($2000 km^2 day^{-1} \approx 23000 m^2\ s^{-1}$)). At a more regional scale, it is interesting to note that it closely matches *Mariano et al.* [2016]'s and *Zavala Sansón et al.* [2018]'s surface drifter-based values for the northern and south-western GoM, respectively ($\approx 10^4 m^2\ s^{-1}$), suggesting that surface diffusivity in the GoM is not only high, but also homogeneous across the basin. Since little observation-based estimates of diffusivity are available at 300 dbar and 1500 dbar, direct comparison with other regions of the ocean is limited. *LaCasce and Bower* [2000] provided estimates of large-scale-saturated relative diffusivity at 5 different sites of the North Atlantic and at different depth ranges. Here, we found saturation values for relative diffusivity of $\approx$9000 and $\approx$4000 $m^2\ s^{-1}$ at 300 and 1500 dbar, respectively. These are small in comparison to *LaCasce and Bower* [2000]'s values in the [100-900 m] range in

the North Atlantic drift off Newfoundland, and at 700 m offshore of the Gulf Stream's eastern flank (≈30000 and ≈40000 $m^2\ s^{-1}$, respectively). Our estimate of the 1500 dbar maximum relative diffusivity is however of the same order of magnitude as at 1000 m in the Mediterranean Outflow and at 1300 m in the Gulf Stream region (≈ $6000m^2\ s^{-1}$).

Most importantly, our results highlight the depth dependence of relative dispersion on scales of [6-150 km] from floats that were released simultaneously at all depths. The DWDE experiment thus provides one of the first estimates of the variation of relative diffusivity with depth at the same time and place. We found that, averaging over all separation scales, relative diffusivity at 300 dbar is about half that at the surface, while it was about 5 time smaller at 1500 dbar. The seemingly scale independence of the ratio of subsurface to surface diffusivity may result from the similar growth law of relative diffusivity with separation scale ($\propto D^{4/3}$) at all depths in the [10-100 km] range, but remains uncertain given the noise level.

While the relationship between relative diffusivity and separation scale seems straightforward and indicative of a Richardson's regime at all scales smaller than O(100 km) and a Rayleigh regime at larger scales (once diffusivity saturates), examination of the other variables complicates the picture. As repeatedly reported in the literature, Lagrangian diagnoses from real ocean observations offer an incomplete description of the turbulent regimes when looked at separately, and sometimes yield contradictory information when compared to one another. This is particularly true when comparing time dependent variables, such as relative dispersion or Kurtosis, with separation scale dependent variables such as relative diffusivity or FSLE [*Beron-Vera and LaCasce*, 2016]. More specifically, the Gulf of Mexico violates two important assumptions of the 2D turbulence theory: the domain is bounded and is not large compared to the scale of the energetic eddies (a typical Loop Current Ring (LCR) can reach 300 km in diameter [*Meunier et al.*, 2018], while the meridional extension of the basin is of about 900 km.), and the turbulence is not stationary, as episodic LCR shedding likely modifies the western basin's dynamical properties in the surface layer as the eddies reach the continental shelf and split into numerous smaller eddies[*Biggs et al.*, 1996; *Lipphardt et al.*, 2008], and in the deep layer as the dipole travelling below the LCR reaches the continental slope [*Tenreiro et al.*, 2018] .

The closed-basin constraint was shown to be an important limiting factor when trying to infer turbulent regimes from relative diffusivity. [*Artale et al.*, 1997] showed that, in that case, the use of FSLEs was more accurate to discriminate between possible

regimes, and this method was successfully applied to infer the regime shift between non-local (Lundgren) and local (Richardson) in a number of studies [*Lacorata et al.*, 1999; *LaCasce and Ohlmann*, 2003; *LaCasce*, 2008]. Here, while the relationship between relative dispersion and time and between relative diffusivity and separation do not show any evidence of a Lundgren regime at short time and space scales (no exponential growth of the former nor D^2 growth of the latter), FSLEs suggest the opposite. At the surface and 300 dbar, FSLEs are nearly constant at small scales, and shift towards a $D^{-2/3}$ law at scales greater than 50 km, and a similar pattern is observed at separations of O(15 km) at 1500 dbar. This suggests the dominance of non-local dispersion at the surface and subsurface at scales smaller than the first baroclinic Rossby radius (50 km in the GoM [*Hamilton et al.*, 2018]), gradually shifting towards local dispersion at greater scales. It also suggests that the size of the energy-containing eddies, which should scale as the separation scale of the regime shift, is approximately 3 times smaller at 1500 m than at near-surface. The short time exponential growth of the Kurtosis ($t < 2$ days), is also consistent with the existence of a Lundgren regime at all depths.

At scales larger than the deformation radius, but still small enough compared to the basin's size [50-100 km], the growth of relative dispersion was shown to follow a power law with exponents decreasing with increasing depth. At the surface, the growth was nearly cubic ($D^2 \propto t^{2.6}$), as expected from Richardson's regime, while at 1500 dBar, it was more consistent with ballistic dispersion ($D^2 \propto t^{2.2}$) [*LaCasce*, 2008] (possibly driven by the boundary current along the shelf). The slope of the FSLEs at these separation scales ($\propto D^{-2/3}$) however supports the hypothesis of a Richardson regime, rather than ballistic dispersion, at all depths.

Because the boundary of enclosed basins can limit the dispersion of particles before the full de-correlation of particle velocities naturally yields a regime shift towards standard diffusion (Rayleigh regime), the long time and large scale limit of the dispersion properties in the GoM deserves further discussion. A transition towards a linear growth of relative dispersion was evident at all depths, suggesting a regime shift from Richardson or ballistic towards Rayleigh. The saturation of relative diffusivity at scales of [100-150 km] also supports this possibility. However, recent work from *Flores Ramírez and Zavala Sansón* [2019] showed that bounded domains could result in a saturation regime, where the growth of relative dispersion is limited to an upper bound of R^2 for circular basins with radius R, or $L^2/4$ for squared basins of side L. While such a saturation of dispersion

should be accompanied by a collapse of relative diffusivity, which is not observed here, the maximum observed surface dispersion after 150 days nearly reaches the saturation dispersion, considering the western GoM as a circular basin of radius $R = 450km$. More strikingly, the Kurtosis at the surface and at 300 dbar closely follow the theoretical saturation Kurtosis (1.67) after 100 days, at least suggesting saturating effects of the basin's geometry.

The peculiarities of the GoM's geometry and intermittent dynamics may not allow a direct generalization of our results to the variation of dispersion with depth in the ocean in general. New experiments, in a larger and open basin would be useful. Such experiments should include an increased number of sampled depths, from the sea-floor to the surface to assess more accurately the vertical distribution of diffusivity in oceanic turbulence.

Acknowledgments

We appreciate early discussions with Luis Zavala Sanson, Joe LaCasce and Javier Berón Vera about dispersion theory. This research has been funded by the Mexican National Council for Science and Technology - Mexican Ministry of Energy - Hydrocarbon Fund, project 201441. This is a contribution of the Gulf of Mexico Research Consortium (CIGoM). We acknowledge PEMEX's specific request to the Hydrocarbon Fund to address the environmental effects of oil spills in the Gulf of Mexico. Drifter and RAFOS float data available for non-profit academic use at https://zenodo.org/record/3979964

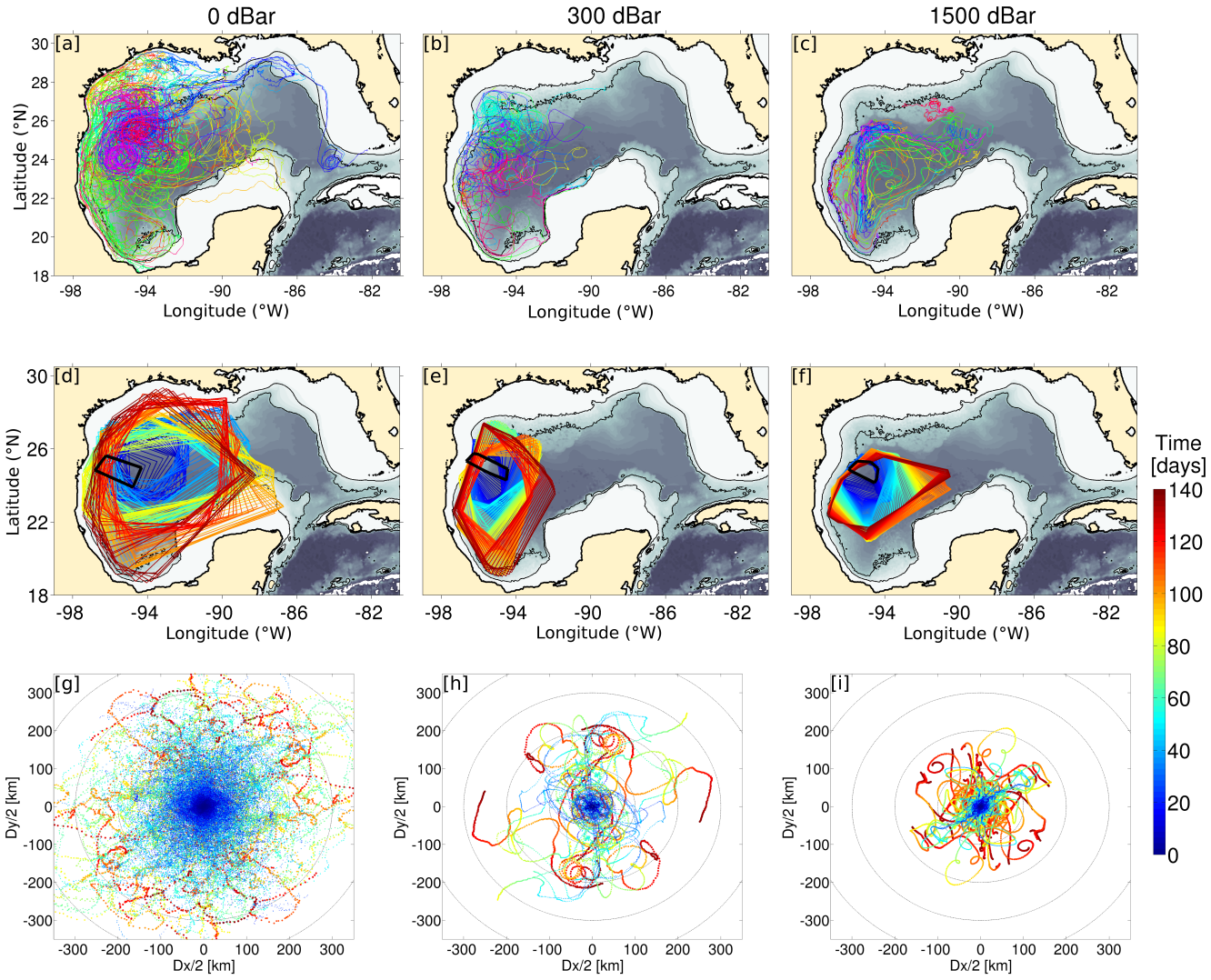

Figure 1. a: Spaghetti plot of the surface drifters trajectories during the whole experiment. b: Same as (a) for the 300 dbar RAFOS floats. c: same as (a) for the 1500 dbar RAFOS floats. d: Smallest convex polygons containing the entire surface drifters set during the first 150 days. Time is colour-coded. The black polygon represents the launching area. e: same as (d) for the 300 dbar RAFOS floats. f: same as (d) for the 1500 dbar RAFOS floats. g: Relative displacements of surface drifters pairs during the first 150 days. Position is referenced to the centre of gravity of each pair and time is colour-coded. Circles are plotted every 100 km. h: same as (g) for the 300 dbar RAFOS floats. i: same as (g) for the 1500 dbar RAFOS floats

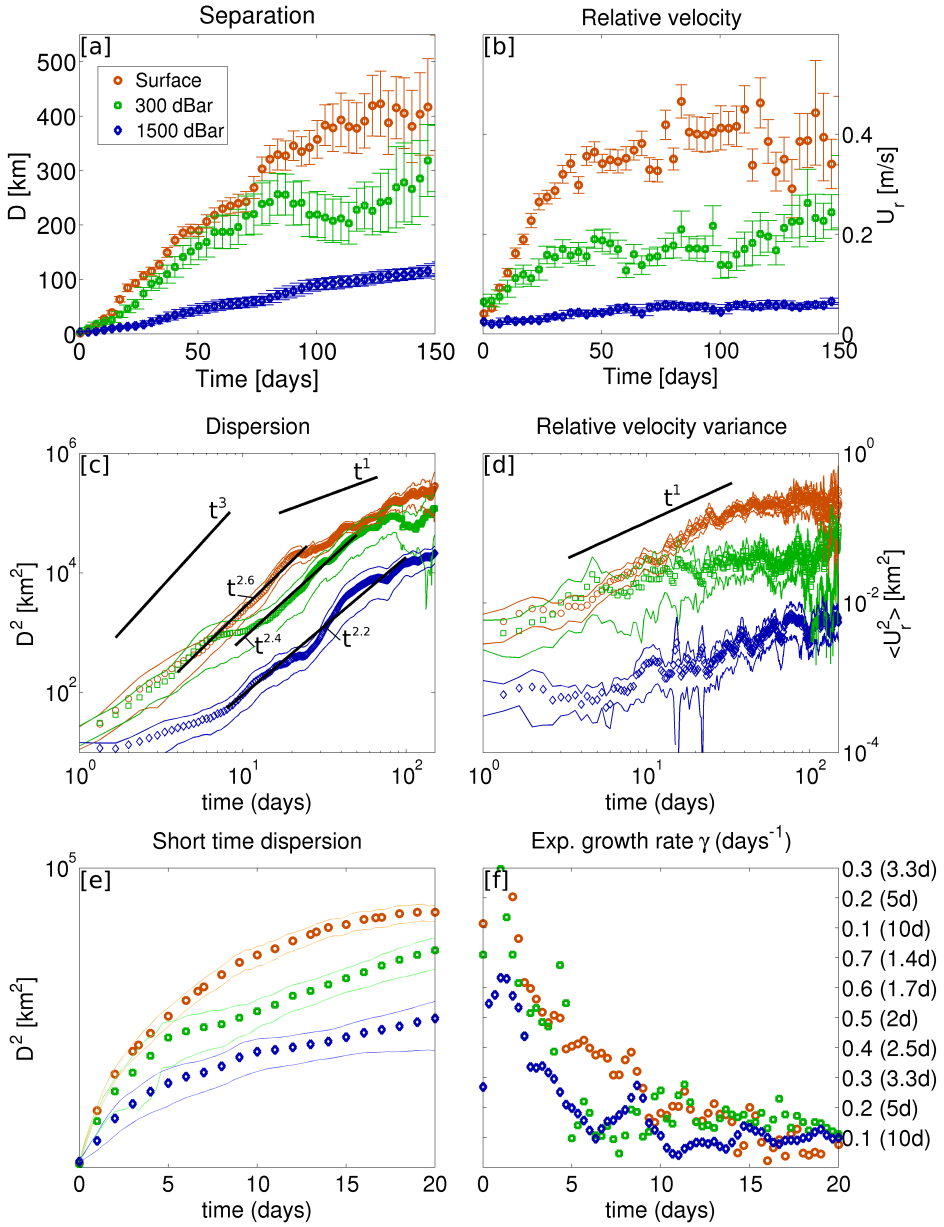

Figure 2. a: Pair separation against time for the surface drifters (orange circles), 300 dbar (green squares), and 1500 dbar RAFOS floats (blue diamonds). b: same as (a) for pair separation velocity. c: Dispersion against time (logarithmic scale). The black lines represent the local linear fit at each depth and a linear and cubic growth, respectively. d: same as (c) for the mean squared pair separation velocity. e: Short time dispersion against time. The time scale is linear while the dispersion scale is logarithmic. The fitted straight lines represent periods of exponential growth. The corresponding e-folding time is also indicated f: Exponential growth rate $\gamma(t)$ (defined as $\gamma(t) = \frac{ln(D^2(t+\delta t))-ln(D^2(t-\delta t))}{2\delta t}$). Pure exponential growth would materialize as periods of constant growth rate. The corresponding e-folding times are provided in parenthesis on the y-axis.

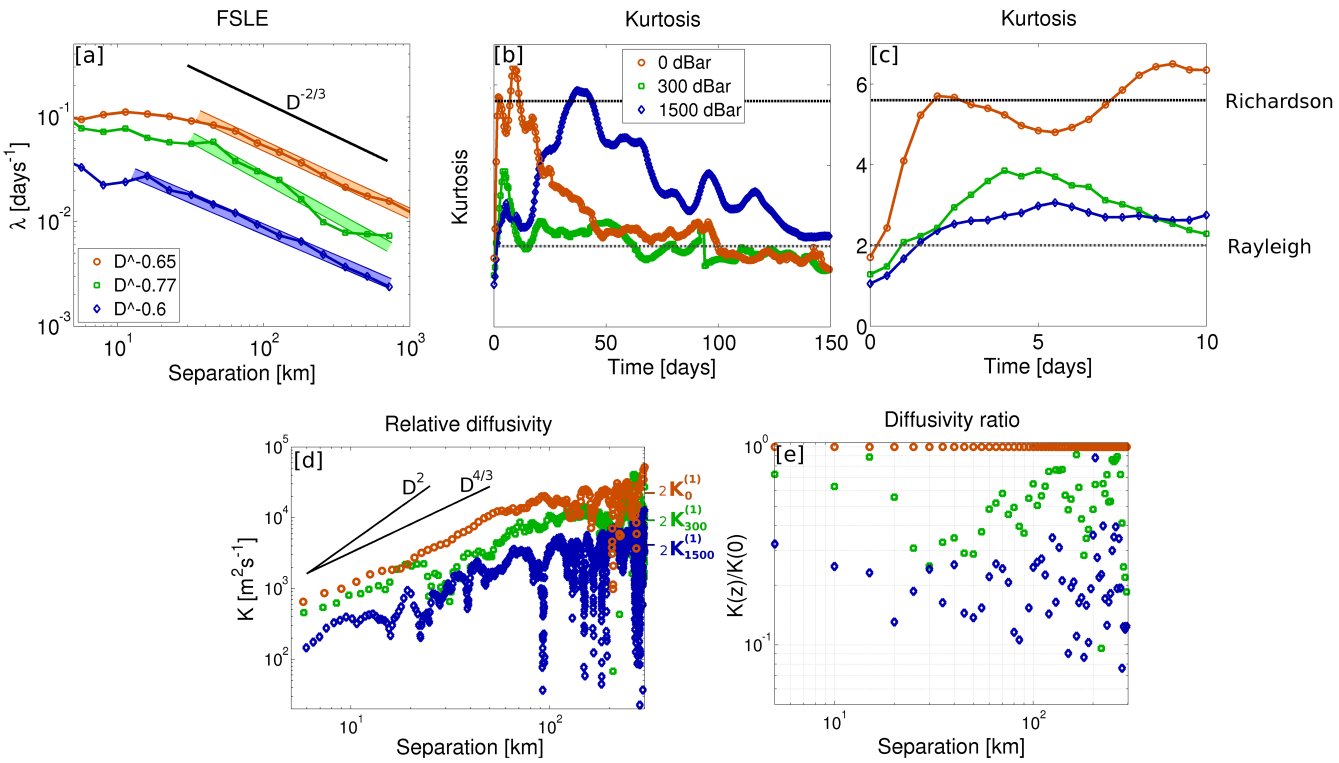

Figure 3. a: Finite size Lyapunov exponents (FSLE, equation 4) against separation scale. The thick lines represent the decay laws indicated in the text boxes. The latter were computed using linear regression. The $D^{-2/3}$ decay law is indicated by the thick black line. b: Kurtosis of the separation probability density function (PDF) against time for the first 150 days. The black dashed line represent the theoretical Kurtosis for the Richardson regime (5.6), while the dashed grey line represent the Kurtosis of the Rayleigh regime (2). c: Same as (b) for the first 10 days. d: Relative diffusivity against separation scale for the surface (orange circles), 300 dbar (green squares), and 1500 dbar (blue diamonds) data sets. The D^2 and $D^{4/3}$ growth laws are plotted as black lines. e: Ratio of the 300 dbar (green) and 1500 dbar (blue) relative diffusivity and the surface relative diffusivity.

References

Artale, V., G. Boffetta, A. Celani, M. Cencini, and A. Vulpiani (1997), Dispersion of passive tracers in closed basins: Beyond the diffusion coefficient, *Physics of Fluids*, *9*(11), 3162–3171, doi:10.1063/1.869433.

Babiano, A., C. Basdevant, P. Le Roy, and R. Sadourny (1990), Relative dispersion in two-dimensional turbulence, *Journal of Fluid Mechanics*, *214*, 535–557, doi:10.1017/S0022112090000258.

Balwada, D., J. H. LaCasce, and K. G. Speer (2016), Scale-dependent distribution of kinetic energy from surface drifters in the Gulf of Mexico, , *43*(20), 10,856–10,863, doi:10.1002/2016GL069405.

Balwada, D., J. H. LaCasce, K. Speer, and R. Ferrari (2019), Relative dispersion in the antarctic circumpolar current.

Batchelor, G. K. (1952), Diffusion in a field of homogeneous turbulence, *Proceedings of the Cambridge Philosophical Society*, *48*(2), 345, doi:10.1017/S0305004100027687.

Bennett, A. F. (1987), A Lagrangian Analysis of Turbulent Diffusion (Paper 6R0783), *Reviews of Geophysics*, *25*, 799, doi:10.1029/RG025i004p00799.

Bennett, A. F., and K. L. Denman (1985), Phytoplankton patchiness: inferences from particle statistics, *Journal of Marine Research*, *43*(2), 307–335.

Beron-Vera, F. J., and J. H. LaCasce (2016), Statistics of Simulated and Observed Pair Separations in the Gulf of Mexico, *Journal of Physical Oceanography*, *46*(7), 2183–2199, doi:10.1175/JPO-D-15-0127.1.

Biggs, D. C., G. S. Fargion, P. Hamilton, and R. R. Leben (1996), Cleavage of a Gulf of Mexico Loop Current eddy by a deep water cyclone, , *101*, 20,629–20,642, doi:10.1029/96JC01078.

Colin de Verdiere, A. (1983), Lagrangian eddy statistics from surface drifters in the eastern north atlantic, *Journal of Marine Research*, *41*(3), 375–398.

Davis, R. E. (1991), Lagrangian ocean studies, *Annual Review of Fluid Mechanics*, *23*, 43–64, doi:10.1146/annurev.fl.23.010191.000355.

Drazen, J. C., C. R. Smith, K. M. Gjerde, S. H. D. Haddock, G. S. Carter, C. A. Choy, M. R. Clark, P. Dutrieux, E. Goetze, C. Hauton, and others (2020), Opinion: Midwater ecosystems must be considered when evaluating environmental risks of deep-sea mining, *Proceedings of the National Academy of Sciences*, *117*(30), 17,455–17,460.

Flores Ramírez, L. M., and L. Zavala Sansón (2019), Two-dimensional turbulence dispersion in a closed domain: Influence of confinement and geometry, *AIP Advances*, *9*(3), 035302, doi:10.1063/1.5081848.

Hamilton, P., R. Leben, A. Bower, H. Furey, and P. Pérez-Brunius (2018), Hydrography of the Gulf of Mexico Using Autonomous Floats, *Journal of Physical Oceanography*, *48*(4), 773–794, doi:10.1175/JPO-D-17-0205.1.

Koszalka, I., J. H. LaCasce, and K. A. Orvik (2009), Relative dispersion in the nordic seas, *Journal of Marine Research*, *67*(4), 411–433.

Kraichnan, R. H. (1967), Inertial Ranges in Two-Dimensional Turbulence, *Physics of Fluids*, *10*(7), 1417–1423, doi:10.1063/1.1762301.

Kujawinski, E. B., M. C. Kido Soule, D. L. Valentine, A. K. Boysen, K. Longnecker, and M. C. Redmond (2011), Fate of Dispersants Associated with the Deepwater Horizon Oil Spill, *Environmental Science and Technology*, *45*(4), 1298–1306, doi:10.1021/es103838p.

LaCasce, J. H. (2008), Statistics from Lagrangian observations, *Progress in Oceanography*, *77*(1), 1–29, doi:10.1016/j.pocean.2008.02.002.

LaCasce, J. H., and A. Bower (2000), Relative dispersion in the subsurface north atlantic, *Journal of marine research*, *58*(6), 863–894.

LaCasce, J. H., and C. Ohlmann (2003), Relative dispersion at the surface of the gulf of mexico, *Journal of Marine Research*, *61*(3), 285–312.

LaCasce, J. H., R. Ferrari, J. Marshall, R. Tulloch, D. Balwada, and K. Speer (2014), Float-Derived Isopycnal Diffusivities in the DIMES Experiment, *Journal of Physical Oceanography*, *44*(2), 764–780, doi:10.1175/JPO-D-13-0175.1.

Lacorata, G., E. Aurell, and A. Vulpiani (1999), Drifters dispersion in the Adriatic Sea: Lagrangian data and chaotic model, *arXiv e-prints*, chao-dyn/9902014.

Lin, J.-T. (1972), Relative Dispersion in the Enstrophy-Cascading Inertial Range of Homogeneous Two-Dimensional Turbulence., *Journal of Atmospheric Sciences*, *29*(2), 394–395, doi:10.1175/1520-0469(1972)029<0394:RDITEC>2.0.CO;2.

Lipphardt, B., A. Poje, A. Kirwan, L. Kantha, and M. Zweng (2008), Death of three loop current rings, *Journal of Marine Research*, *66*(1), 25–60.

Lundgren, T. S. (1981), Turbulent pair dispersion and scalar diffusion, *Journal of Fluid Mechanics*, *111*, 27–57, doi:10.1017/S0022112081002280.

Mariani, P., B. MacKenzie, A. Visser, and V. Botte (2007), Individual-based simulations of larval fish feeding in turbulent environments, *Marine Ecology Progress Series*, *347*,

155–169, doi:10.3354/meps07092.

Mariano, A. J., E. H. Ryan, H. S. Huntley, L. C. Laurindo, E. Coelho, A. Griffa, T. M. Özgökmen, M. Berta, D. Bogucki, S. S. Chen, M. Curcic, K. L. Drouin, M. Gough, B. K. Haus, A. C. Haza, P. Hogan, M. Iskandarani, G. Jacobs, A. D. Kirwan, N. Laxague, B. Lipphardt, M. G. Magaldi, G. Novelli, A. Reniers, J. M. Restrepo, C. Smith, A. Valle-Levinson, and M. Wei (2016), Statistical properties of the surface velocity field in the northern Gulf of Mexico sampled by GLAD drifters, *Journal of Geophysical Research (Oceans)*, *121*(7), 5193–5216.

McNutt, M. K., R. Camilli, T. J. Crone, G. D. Guthrie, P. A. Hsieh, T. B. Ryerson, O. Savas, and F. Shaffer (2012), Review of flow rate estimates of the Deepwater Horizon oil spill, *Proceedings of the National Academy of Science*, *109*(50), 20,260–20,267, doi:10.1073/pnas.1112139108.

Meunier, T., E. Pallás-Sanz, M. Tenreiro, E. Portela, J. L. Ochoa, A. Ruíz-Angulo, and S. Cusí (2018), The Vertical Structure of a Loop Current Eddy, *Manuscript submitted for publication*.

Morel, P., and M. Larceveque (1974), Relative Dispersion of Constant-Level Balloons in the 200-mb General Circulation., *Journal of Atmospheric Sciences*, *31*(8), 2189–2196, doi:10.1175/1520-0469(1974)031<2189:RDOCBI>2.0.CO;2.

North, E. W., E. E. Adams, Z. Schlag, C. R. Sherwood, R. He, K. H. Hyun, and S. A. Socolofsky (2011), Simulating Oil Droplet Dispersal From the Deepwater Horizon Spill With a Lagrangian Approach, *Washington DC American Geophysical Union Geophysical Monograph Series*, *195*, 217–226, doi:10.1029/2011GM001102.

Ollitrault, M., C. Gabillet, and A. C. de Verdière (2005), Open ocean regimes of relative dispersion, *Journal of Fluid Mechanics*, *533*, 381–407.

Poje, A. C., T. M. Özgökmen, J. Lipphardt, Bruce L., B. K. Haus, E. H. Ryan, A. C. Haza, G. A. Jacobs, A. J. H. M. Reniers, M. Josefina Olascoaga, G. Novelli, A. Griffa, F. J. Beron-Vera, S. S. Chen, E. Coelho, P. J. Hogan, J. Kirwan, Albert D., H. S. Huntley, and A. J. Mariano (2014), Submesoscale dispersion in the vicinity of the Deepwater Horizon spill, *Proceedings of the National Academy of Science*, *111*(35), 12,693–12,698, doi:10.1073/pnas.1402452111.

Poje, A. C., T. M. Ã-zgökmen, D. J. Bogucki, and A. D. Kirwan (2017), Evidence of a forward energy cascade and Kolmogorov self-similarity in submesoscale ocean surface drifter observations, *Physics of Fluids*, *29*(2), 020701, doi:10.1063/1.4974331.

Reddy, C. M., J. S. Arey, J. S. Seewald, S. P. Sylva, K. L. Lemkau, R. K. Nelson, C. A. Carmichael, C. P. McIntyre, J. Fenwick, G. T. Ventura, B. A. S. Van Mooy, and R. Camilli (2012), Composition and fate of gas and oil released to the water column during the Deepwater Horizon oil spill, *Proceedings of the National Academy of Science*, *109*(50), 20,229–20,234, doi:10.1073/pnas.1101242108.

Tenreiro, M., J. Candela, E. P. Sanz, J. Sheinbaum, and J. Ochoa (2018), Near-Surface and Deep Circulation Coupling in the Western Gulf of Mexico, *Journal of Physical Oceanography*, *48*(1), 145–161, doi:10.1175/JPO-D-17-0018.1.

van Sebille, E., M. H. England, and G. Froyland (2012), Origin, dynamics and evolution of ocean garbage patches from observed surface drifters, *Environmental Research Letters*, *7*(4), 044040, doi:10.1088/1748-9326/7/4/044040.

Zavala Sansón, L. (2015), Surface dispersion in the Gulf of California, *Progress in Oceanography*, *137*, 24–37, doi:10.1016/j.pocean.2015.04.008.

Zavala Sansón, L., J. Sheinbaum, and P. Pérez-Brunius (2018), Single-particle statistics in the southern gulf of mexico, *Geofísica internacional*, *57*(2), 139–150.

Zhurbas, V., and I. Oh (2004), Drifter-derived maps of lateral diffusivity in the pacific and atlantic oceans in relation to surface circulation patterns, *Journal of Geophysical Research (Oceans)*, *109*(C5), C05015, doi:10.1029/2003JC002241.

Figure 1.

0 dBar

300 dBar

1500 dBar

[a]

[b]

[c]

[d]

[e]

[f]

[g]

[h]

[i]

Latitude (°N)

Longitude (°W)

Dy/2 [km]

Dx/2 [km]

Time [days]

Figure 2.

Separation

[a]

Surface
300 dBar
1500 dBar

D [km]

Time [days]

Relative velocity

[b]

U_r [m/s]

Time [days]

Dispersion

[c]

t^1
t^3
$t^{2.6}$
$t^{2.4}$
$t^{2.2}$

D^2 [km^2]

time (days)

Relative velocity variance

[d]

t^1

$\langle U_r^2 \rangle$ [km^2]

time (days)

Short time dispersion

[e]

D^2 [km^2]

time (days)

Exp. growth rate γ (days^{-1})

[f]

0.3 (3.3d)
0.2 (5d)
0.1 (10d)
0.7 (1.4d)
0.6 (1.7d)
0.5 (2d)
0.4 (2.5d)
0.3 (3.3d)
0.2 (5d)
0.1 (10d)

time (days)

Figure 3.

FSLE

[a]

$D^{-2/3}$

λ [days^{-1}]

10^{-1}

10^{-2}

10^{-3}

D^-0.65

D^-0.77

D^-0.6

10^{1} 10^{2} 10^{3}

Separation [km]

Kurtosis

[b]

0 dBar

300 dBar

1500 dBar

Kurtosis

0 50 100 150

Time [days]

Kurtosis

[c]

6

4

2

0

Richardson

Rayleigh

0 5 10

Time [days]

Relative diffusivity

[d]

D^{2}

$D^{4/3}$

K [m^{2}s^{-1}]

10^{5} 10^{4} 10^{3} 10^{2}

$2K_0^{(1)}$

$2K_{300}^{(1)}$

$2K_{1500}^{(1)}$

10^{1} 10^{2}

Separation [km]

Diffusivity ratio

[e]

K(z)/K(0)

10^{0} 10^{-1}

10^{1} 10^{2}

Separation [km]